Brodogradnja/Shipbuilding/Open access

Volume 71 Number 3, 2020

Xiaoyang Lu
Zhiquan Liu
Zhenzhong Chu

http://dx.doi.org/10.21278/brod71305

ISSN 0007-215X
eISSN 1845-5859

NONLINEAR ADAPTIVE HEADING CONTROL FOR AN UNDERACTUATED SURFACE VESSEL WITH CONSTRAINED INPUT AND SIDESLIP ANGLE COMPENSATION

UDC 629.5.072.4
Original scientific paper

Summary

In this paper, a nonlinear adaptive heading controller is developed for an underactuated surface vessel with constrained input and sideslip angle compensation. The controller design is accomplished in a framework of backstepping technique. First, to amend the irrationality of the traditional definition of the desired heading, the desired heading is compensated by the sideslip angle. Considering the actuator physical constrain, a hyperbolic tangent function and a Nussbaum function are introduced to handle the nonlinear part of control input. The error and the disturbance are estimated and compensated by an adaptive control law. In addition, to avoid the complicated calculation of time derivatives of the virtual control, the command filter is introduced to integrate with the control law. It is analysed by the Lyapunov theory that the closed loop system is guaranteed to be uniformly ultimately bounded stability. Finally, the simulation studies illustrate the effectiveness of the proposed control method.

Key words: *heading control; adaptive control; backstepping; sideslip; input saturation*

1. Introduction

Marine mechatronic systems play an important role in modern industrial manufacturing. As a basic problem in the field of the vessel control, the heading control has always been a research focus. Many advanced control methods have been applied to the vessel control, but there are still many disadvantages. An adaptive output feedback control method was proposed to address uncertainties and external disturbances of a vessel without hydrodynamic structure information, but it ran with a slow calculation speed and expensive online equipment [1,2]. Zhang and Zhang used a feedback linearization algorithm to avoid complicated proofs, but the input saturation was not considered and a high precision model was required [3]. A fuzzy adaptive method was developed to investigate disturbances and uncertainty attenuation, but the control rules were usually difficult to determine and optimize [4,5]. Because of its reliable and stable, PID control method has been widely used. With the progress of technology, traditional PID controller cannot satisfy the improvement of control quality requirements. So intelligent control algorithms were introduced and combined with PID in the field of the

vessel control [6]. Backstepping control introduces additional nonlinearity into the control process to eliminate undesirable nonlinearity in the system. It is one of the most popular control design techniques. The backstepping technique was more commonly used in full-actuated vessels rather than underactuated vessels, however, traditional surface vessels are usually underactuated [7-10].

Whether vessels are full-actuated or underactuated, input saturation is a common phenomenon in practical systems. The Input of actuator will enter a saturated state, when it reaches a certain limit. The saturation of actuator will reduce the system performance and even lead to the instability of the closed loop system. Therefore, it is necessary to consider saturation in the design of marine vehicle control systems. The adaptive neural network (NN) control method was presented by using a Gaussian error function [11]. It tackled the discontinuous and differentiable problem of non-smooth asymmetric saturation effectively. The interval type-2 fuzzy system and an observer based on strictly positive real (SPR) theory were employed to handle the effect of unknown asymmetric saturations nonlinearity [12]. The auxiliary system was adopted to handle the influence of input saturation and states of the system were used to design the controller [13]. In order to tackle the potential unstable behaviour caused by the saturation of rudders, an adaptive fuzzy compensator was introduced in an autonomous underwater vehicle (AUV) bottom following control system [14].To satisfy the input saturation of the control system, Huang and Sharma built a new state-dependent coefficient (SDC) matrix to express the relationship between different variables [7]. This method could maintain the heading accurately and was used for the vessel dynamic positioning control system [15,16]. Note that the influence of nonzero sideslip angle was not considered in the above references.

The sideslip angle plays an important role for marine surface vessel control. The desired heading is usually chosen by the tangent direction of the path, with the assumption that the nonzero sideslip angle is ignored, the actual sailing direction of the vessel is not consistent with the tangent direction. Therefore, the traditional definition of the desired heading may lead to the deviation of the heading. However, the sideslip angle is time-varying which can be influenced by environmental disturbances, such as the currents, waves and winds. To handle the sideslip angle problem, an extended state observer was designed to estimate the sideslip angle timely and exactly [17,18]. It was contributed to track the desired path accurately regardless of constant ocean disturbances. An adaptation law was adopted to estimate and compensate the unknown sideslip angle considered as a constant parameter [19, 20]. Nie and Lin proposed the fuzzy adaptive integral line-of-sight (FAILOS) guidance law which was established with the adaptive fuzzy logic system. This method calculated the desired heading and compensated the sideslip angle effectively [21]. In [22], the ship course-keeping control was achieved with the sideslip angle compensation, but the global positioning system (GPS) and rate gyroscope sensors were needed. For nonlinear characteristics, input saturation and external disturbances of an underactuated vessel motion control system, a robust adaptive backstepping heading controller with constrained input and sideslip angle compensation is designed. The main contributions in this paper are summarized as follows.

- For input saturation, the hyperbolic tangent function is used to approximate the constraints. An adaptive control law is designed to handle the approximation error along with the external disturbance in the yaw direction;
- By introducing the command filter, the tedious analytical calculation of the time derivative of the virtual control law is avoided, which simplifies the backstepping procedure.
- Combining the above points, the heading controller is developed based on the backstepping method. The heading error can be uniformly ultimately bounded (UUB) and all states of the closed-loop system are bounded.

This paper is organized as follows. The section 2 describes the vessel dynamics and related disturbances. The section 3 gives the control objectives. The section 4 amends the desired heading and designs the nonlinear robust adaptive heading controller. The simulation results are explained in the section 5 and the conclusion is expressed in the section 6.

2. Problem statement

2.1 Dynamics of the underactuated surface vessel

Assuming the vessel has a xz plane of symmetry; the heave, roll and pitch motions can be neglected. To simplify the vessel model and facilitate the design of controller, the surge velocity u is assumed to be a constant and the sway velocity v is assumed to passive bounded [23, 24]. Based on these assumptions, the dynamic model of the underactuated surface vessel (USV) can be simplified to a 2 degree of freedom (DOF) model (i.e. in the direction of sway and yaw) and it is described as follows [25]:

$$\begin{cases} \dot{r} = \dfrac{(m_{11}-m_{22})}{m_{33}} u_r v_r + f_1(r) + \dfrac{1}{m_{33}} \tau_r(\varphi) + \omega_r \\ \dot{v}_r = -\dfrac{m_{11}}{m_{22}} u_r r + f_2(v) + \dfrac{1}{m_{22}} (-\sin(\psi)\omega_{v1} + \cos(\psi)\omega_{v2}) \\ \dot{\psi} = r \end{cases} \tag{1}$$

where ψ denotes the heading angle of the vessel in the earth fixed frame OX_oY_o, shown in Fig.1; u_r, v_r, r represent the vessel surge velocity, sway velocity and yaw rate coordinated in the body fixed frame BX_bY_b, respectively. The parameters m_{11}, m_{22}, m_{33} stand for the vessel inertia including added masses in the surge, sway and yaw; the damping functions $f_1(r)$, $f_2(v)$ are formulated as follows:

$$f_1(r) = -\frac{d_{r1}}{m_{33}} r - \frac{1}{m_{33}} (d_{r2} r^2 \tanh(\frac{r}{\lambda}) + d_{r3} r^3) \tag{2}$$

$$f_2(v) = -\frac{d_{v1}}{m_{22}} v_r - \frac{1}{m_{22}} (d_{v2} {v_r}^2 \tanh(\frac{v_r}{\lambda}) + d_{v3} {v_r}^3) \tag{3}$$

where d_{ri}, d_{vi} are the hydrodynamic damping coefficients in the yaw and sway axes for $i = 1,2,3$, respectively. λ is a small positive constant. The rudder moment φ is the only control input of the USV, which is calculated actually. Considering the input constraint [26], the new input $\tau_r(\varphi)$ is the output of the saturator and described by

$$\tau_r(\varphi) = \begin{cases} \text{sign}(\varphi)\tau_M, & |\varphi| \geq \tau_M \\ \varphi, & |\varphi| < \tau_M \end{cases} \tag{4}$$

where $\tau_M > 0$ represents the known bound of τ_r. ω_r, ω_{vi} ($i = 1,2$) denote unknown but bounded time varying disturbances in the yaw and sway direction. V_c and β_c are the current speed and angle in the earth fixed frame OX_oY_o, respectively. Then

$[u_c\ v_c\ 0]^{\mathrm{T}} = [V_c\cos(\beta_c-\psi)\ \ V_c\sin(\beta_c-\psi)\ \ 0]^{\mathrm{T}}$ is the current velocity coordinated in the body fixed frame. $[u\ v\ r]^{\mathrm{T}}$ and $[u_r\ v_r\ r]^{\mathrm{T}}$ stand for the actual velocity and relative velocity of the vessel with respect to the body fixed frame, respectively. The relationship between them is defined as $[u_r\ v_r\ r]^{\mathrm{T}} = [u\ v\ r]^{\mathrm{T}} - [u_c\ v_c\ 0]^{\mathrm{T}}$.

Thus, considering the effect of the current on the vessel without using GPS equipment, the sideslip angle can be obtained by

$$\beta = \arctan\frac{v}{u} = \arctan\frac{v_r + V_c\sin(\beta_c-\psi)}{u_r + V_c\cos(\beta_c-\psi)} \tag{5}$$

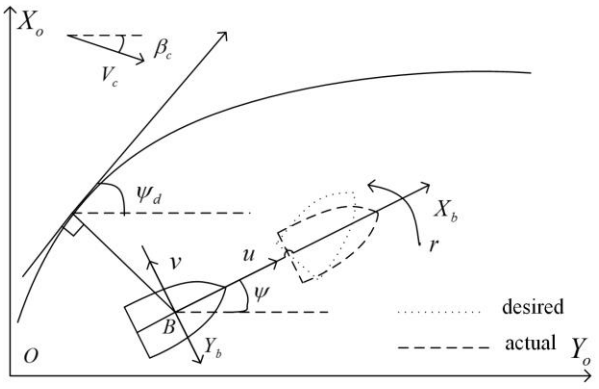

Fig. 1 The traditional desired heading

2.2 Wave model

Among many possible external disturbances acting on vessels, the waves are extremely important, which have an impact on the heading control performance. Therefore, the wave is considered as the disturbance ω_r in the yaw direction. The wave model is given as

$$y(s) = h(s)\omega(s) \tag{6}$$

where $\omega(s)$ stands for a zero mean Gauss white noise process with a power spectral density equal to 0.1. And $h(s)$ is a transfer function of the second order wave, described by

$$h(s) = \frac{K_\omega s}{s^2 + 2\zeta\omega_0 s + {\omega_0}^2} \tag{7}$$

where $\omega_0 = 4.85/T_\omega$, $K_\omega = 2\zeta\omega_0\sigma_m$, $\sigma_m = \sqrt{0.0185T_\omega h_{1/3}}$, ω_0 and σ_m denote the wave frequency and the wave intensity, respectively. ζ represents a damping coefficient, K_ω is a constant that expresses gain.

2.3 Control Objective

Backstepping method requires that functions can be differentiated in the process of derivation of virtual control variables, while saturation function $\tau_r(\varphi)$ is not a smooth curve. To use the backstepping method to develop the heading controller, we divide $\tau_r(\varphi)$ into two parts, which can be given as $\tau_r(\varphi) = \mathrm{g}(\varphi) + \mu(\varphi)$ [27], and a smooth function $g(\varphi)$ with hyperbolic tangent function is defined to approximate the saturation nonlinearity.

$$g(\varphi) = \text{sign}(\varphi)\tau_M \tanh(\frac{\varphi}{\text{sign}(\varphi)\tau_M}) \tag{8}$$

We define b as the bound of the function $\mu(\varphi)$ and it can be expressed as

$$\begin{aligned} |\mu(\varphi)| &= |\tau_r(\varphi) - \text{g}(\varphi)| \\ &\le \max\{\text{sign}(\varphi)\tau_M(1-\tanh(1)\} \\ &= b \end{aligned} \tag{9}$$

From Equations (4, 8, 9), the plant (1) is redefined as

$$\begin{cases} \dot{r} = \dfrac{(m_{11}-m_{22})}{m_{33}} u_r v_r + f_1(r) + \dfrac{1}{m_{33}} g(\varphi) + \Delta \\ \dot{v}_r = -\dfrac{m_{11}}{m_{22}} u_r r + f_2(v) + \dfrac{1}{m_{22}}(-\sin(\psi)\omega_{v1} + \cos(\psi)\omega_{v2}) \\ \dot{\varphi} = -c\varphi + \phi \\ \dot{\psi} = r \end{cases} \tag{10}$$

where $\Delta = \omega_r + \mu(\varphi)$. Because ω_r and $\mu(\varphi)$ are bounded. Δ is bounded and we assume $|\Delta| \le \sigma$. c is a positive constant. In the new plant (10), it is hard to design the actual input φ directly. Therefore the auxiliary signal ϕ is introduced to develop the controller and analysis the system stability.

The objective is to design a heading control law for (10) with input saturation (8) such that:

- The heading error converges to the neighborhood of a small value;
- The control input moment keeps a small value.

3. Preliminaries

This section gives several definitions and lemmas used in the controller development and the system stability analysis later.

Definition 1: The following Young's inequality holds for any $x \in \mathbb{R}$, $y \in \mathbb{R}$,

$$xy \le \frac{\varepsilon^p}{p}|x|^p + \frac{1}{q\varepsilon^q}|y|^q \tag{11}$$

where $\varepsilon > 0$ and the positive constants p, q satisfy $\frac{1}{p} + \frac{1}{q} = 1$ with $p > 1$, $q > 1$. And the Young's inequality used in this paper is presented as $xy \le \frac{1}{2}x^2 + \frac{1}{2}y^2$

Definition 2: For any $x \in \mathbb{R}$, the hyperbolic tangent function $\tanh(x)$ is expressed as

$$\tanh(x) = \frac{e^x - e^{-x}}{e^x + e^{-x}} \tag{12}$$

Lemma 1 [27]: For $\forall x \in \mathbb{R}$, the following inequality holds

$$0 \le |x| - x\tanh(\frac{x}{\upsilon}) \le \kappa\upsilon \tag{13}$$

where $\upsilon \in \mathbb{R}^+$, $\kappa = e^{-(\kappa+1)}$ with $\kappa = 0.2785$.

Definition 3: A Nussbaum type function $\mathrm{N}(s)$ satisfies the following two properties,

$$\lim_{k\to\pm\infty} \sup \frac{1}{k}\int_0^k \mathrm{N}(s)\,\mathrm{d}s = \infty \tag{14}$$

$$\lim_{k\to\pm\infty} \inf \frac{1}{k}\int_0^k \mathrm{N}(s)\,\mathrm{d}s = -\infty \tag{15}$$

Lemma 2: Define $V(\cdot)$ and $\chi(\cdot)$ as bounded smooth functions on $\left[0, t_f\right)$, with $V(t) \ge 0$, $\forall t \in \left[0, t_f\right)$, then the following inequality holds [28]:

$$V \le V(0)\mathrm{e}^{-ct} + \frac{M}{a}(1-\mathrm{e}^{-ct}) + \frac{\mathrm{e}^{-ct}}{r_\chi}\int_0^t (\varepsilon \mathrm{N}(\chi)-1)\dot{\chi}e^{c\tau}d\tau \tag{16}$$

where $\mathrm{N}(\chi)$ is a Nussbaum type function. a, r_χ, ε, M are positive constants and $\int_0^t (\varepsilon \mathrm{N}(\chi)-1)\dot{\chi}e^{c\tau}d\tau$ are bounded on $\left[0, t_f\right)$.

4. Control design

To deal with the influence of nonzero sideslip angle and the input saturation on the heading control, the following two aspects are shown in this section:

- The desired heading is compensated by the sideslip angle;
- The input saturation function is handled by hyperbolic tangent function and Nussbaum function. The approximation error and disturbances are estimated and compensated by the adaptive law. The command filter is introduced to avoid the complicated calculation. The heading controller is designed based on the backstepping method and the stability of the whole control system is proved.

4.1 Desired heading amendment

In the heading control design, the tangent angle of the desired path is usually chosen as the desired heading angle, which is the traditional definition of heading angle. The sideslip angle is affected by not only steering, but also the ocean current on the vessel. However, the nonzero sideslip angle is seldom considered in the practical design. Especially for the underactuated vessel in this paper, one input is used to control both the yaw rate and sway velocity so that the direction of the vessel's gravity velocity is not coincide with the heading of the vessel, which gradually causes the vessel not following the right course.

To handle this problem, we can use the nonzero sideslip angle to amend the irrationality of the desired heading. Because the desired direction of gravity center velocity differs from the tangent angle of the desired path by a sideslip angle [29]. The amended desired heading and the new heading error for underactuated vessel are proposed, respectively.

The amended desired heading ψ_{da} shown in Fig.2 is presented as

$$\psi_{da} = \psi_d - \beta \tag{17}$$

With the nonzero sideslip angle, the new heading error e_a is given as

$$e_a = \psi - \psi_{da} = \psi - \psi_d + \beta \tag{18}$$

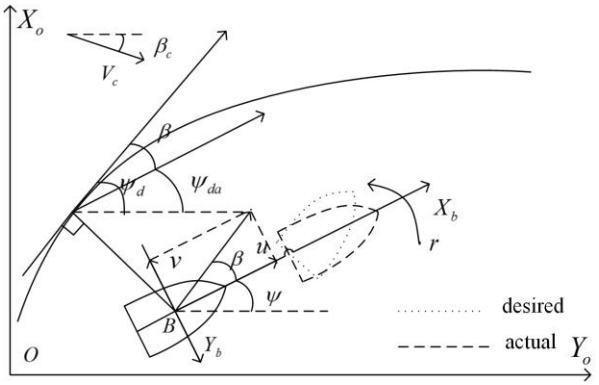

Fig. 2 The amended desired heading

4.2 Controller design

Before the controller is designed, since the backstepping method does not have a good solution to the problems caused by the expansion of terms in the derivative process of virtual control, a command filter is introduced to avoid the complex calculation [30]. The filter shown in Fig.3 can be expressed by

$$\begin{cases} \dot{x}_{1i} = x_{2i} \\ \dot{x}_{2i} = -2\xi_i\omega_i(x_{2i} + \text{sat}(\dfrac{\omega_i^2}{2\xi_i\omega_i}(x_{1i} - \text{sat}(\alpha_{i0})))) \end{cases} \tag{19}$$

where $\alpha_{i0}(i = 1,2)$ denotes the virtual control law, and we can get $\alpha_{i1}=\text{sat}(\dfrac{\omega_i^2}{2\xi_i\omega_i}(x_{1i} - \text{sat}(\alpha_{i0})))$. There are $x_{1i} = \alpha_i$, $x_{2i} = \dot{\alpha}_i$, which α_i and $\dot{\alpha}_i$ are generated from α_{i0} through the system. And $\alpha_i - \alpha_{i0} = \Delta\alpha_i$, it stands for the estimation error of the filter. $\xi_i > 0$ and $\omega_i > 0$ are filter parameters.

$$\text{sat}(\alpha_{ij}) = \begin{cases} \text{sign}(\alpha_{ij})\alpha_{ijm}, & |\alpha_{ij}| \geq \alpha_{ijm} \\ \alpha_{ij}, & |\alpha_{ij}| < \alpha_{ijm} \end{cases} \tag{20}$$

where α_{ijm} is the bound of α_{ij} for $i = 1,2, j = 0,1$. When $\xi_i \geq 1$ (high damping ratio) is chosen, the filter states can converge fast, which attain the input value and its derivative. α_i and $\dot{\alpha}_i$ are limited by virtual control laws.

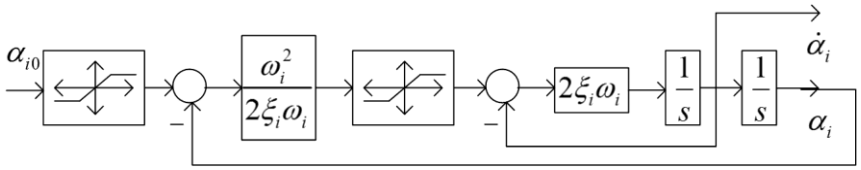

Fig. 3 Configuration of the command filter

Introduce the following new variables to transform states:

$$z_1 = \psi - \psi_{da} = \psi - \psi_d + \beta \tag{21}$$

$$z_2 = r - \alpha_1 \tag{22}$$

$$z_3 = g(\varphi) - \alpha_2 \tag{23}$$

where α_1 and α_2 are the virtual control laws. Considering the plant (10) and the filter, the derivative of z_1, z_2 and z_3 are expressed by

$$\dot{z}_1 = z_2 - \dot{\psi}_d + \dot{\beta} + \alpha_1 \tag{24}$$

$$\dot{z}_2 = \frac{(m_{11} - m_{22})}{m_{33}} u_r v_r - \frac{d_{r1}}{m_{33}} r - \frac{1}{m_{33}} (d_{r2} r^2 \tanh(\frac{r}{\lambda}) + d_{r3} r^3) + \frac{1}{m_{33}} (z_3 + \alpha_2) + \Delta - \dot{\alpha}_1 \tag{25}$$

$$\dot{z}_3 = \frac{\partial g(\varphi)}{\partial \varphi} (-c\varphi + \phi) - \dot{\alpha}_2 \tag{26}$$

Based on the above new definitions, the backstepping method is summarized as the following steps:

Step 1: start with the expression of $\Delta\alpha_1$, from Equation (24), we have

$$\dot{z}_1 = z_2 + \alpha_{10} + \Delta\alpha_1 - \dot{\psi}_d + \dot{\beta} \tag{27}$$

Define an auxiliary design system to solve the effect of the estimation error $\Delta\alpha_1$:

$$\dot{e}_1 = \begin{cases} -k_{e1} e_1 - f_1 e_1 + \gamma_1 \Delta\alpha_1, & |e_1| > \bar{e} \\ 0, & |e_1| \le \bar{e}_1 \end{cases} \tag{28}$$

where $k_{e1} > 1$, $\gamma_1 > 0$ and $\bar{e}_1$ is a small positive constant. f_1 is given as

$$f_1 = \frac{z_1 \Delta\alpha_1 + 0.5\gamma_1^2 \Delta\alpha_1^2}{|e_1|^2} \tag{29}$$

with $|e_1| \neq 0$.

Choose the candidate Lyapunov function (CLF) for step 1 as

$$V_1 = 0.5 z_1^2 + 0.5 e_1^2 \tag{30}$$

With Equations (27-29), the derivative of V_1 satisfies

$$\dot{V}_1 = z_1(z_2 + \alpha_{10} - \dot{\psi}_d + \dot{\beta}) - k_{e1}e_1^2 - 0.5\gamma_1^2\Delta\alpha_1^2 + e_1\gamma_1\Delta\alpha_1 \tag{31}$$

Design this virtual control law as

$$\alpha_{10} = -k_1 z_1 + \dot{\psi}_d - \dot{\beta} + k_{a1}e_1 \tag{32}$$

where k_1 is a positive constant, $k_{a1} > 0$.

Based on the Definition 1, then

$$e_1\gamma_1\Delta\alpha_1 \le 0.5e_1^2 + 0.5\gamma_1^2\Delta\alpha_1^2 \tag{33}$$

$$k_{a1}z_1e_1 \le 0.5k_{a1}^2z_1^2 + 0.5e_1^2 \tag{34}$$

Therefore, we can get

$$\dot{V}_1 \le -(k_1 - 0.5k_{a1})z_1^2 - (k_{e1} - 1)e_1^2 + z_1z_2 \tag{35}$$

Step 2: to handle $\Delta\alpha_2$ like an auxiliary design system in step1, define

$$\dot{e}_2 = \begin{cases} -k_{e2}e_2 - f_2e_2 + \gamma_2\Delta\alpha_2, & |e_2| > \bar{e}_2 \\ 0, & |e_2| \le \bar{e}_2 \end{cases} \tag{36}$$

with $k_{e2} > 1$, $\gamma_2 > 0$. $\bar{e}_2$ is a small positive constant and satisfies $|e_2| \ne 0$, f_2 is given as

$$f_2 = \frac{z_2\Delta\alpha_2 + 0.5\gamma_2^2\Delta\alpha_2^2}{|e_2|^2} \tag{37}$$

For Δ in (10) with assumption $|\Delta| \le \sigma$, we define

$$\tilde{\sigma} = \hat{\sigma} - \sigma \tag{38}$$

where $\hat{\sigma}$, $\tilde{\sigma}$ are the estimation and the estimation error of σ, respectively.

Considering the errors σ and $\Delta\alpha_2$, another CLF can be written as

$$V_2 = V_1 + 0.5m_{33}z_2^2 + 0.5e_2^2 + \frac{0.5}{\gamma_f}\tilde{\sigma}^2 \tag{39}$$

with $\gamma_f > 0$.

It is difficult to obtain the derivative of disturbance directly. Compare with the adaptive law dynamics, the frequency of disturbance changes slowly. Therefore, we have $\dot{\sigma} = 0$.

It leaves the derivative of V_2 from Equations (25, 32, 35, 36, 38) as

$$\begin{aligned}\dot{V}_2 &= \dot{V}_1 + m_{33}z_2\dot{z}_2 + e_2\dot{e}_2 + \frac{1}{\gamma_f}\tilde{\sigma}\dot{\tilde{\sigma}} \\ &\le -(k_1 - 0.5k_{a1})z_1^{\,2} - (k_{e1} - 1)e_1^{\,2} + z_1z_2 + z_2((m_{11} - m_{22})u_rv_r \\ &\quad - d_{r1}r - (d_{r2}r^2\tanh(\frac{r}{\lambda}) + d_{r3}r^3) + (z_3 + \alpha_{20}) + m_{33}\Delta - m_{33}\dot{\alpha}_1) \\ &\quad - k_{e2}e_2^{\,2} - 0.5\gamma_2^{\,2}\Delta\alpha_2^{\,2} + e_2\gamma_2\Delta\alpha_2 + \frac{1}{\gamma_f}\tilde{\sigma}\dot{\hat{\sigma}}\end{aligned} \tag{40}$$

With the aforementioned Lemma1 and $|\Delta| \le \sigma$, we can get

$$m_{33}z_2\Delta \le m_{33}|z_2|\sigma \le m_{33}z_2\tanh(\frac{z_2}{\upsilon})\sigma + m_{33}\kappa\upsilon\sigma \tag{41}$$

At this time, the virtual control law α_{20} can be given as

$$\begin{aligned}\alpha_{20} &= -(m_{11} - m_{22})u_rv_r + d_{r1}r + d_{r2}r^2\tanh(\frac{r}{\lambda}) + d_{r3}r^3 \\ &\quad - z_1 - k_2z_2 + m_{33}\dot{\alpha}_1 - m_{33}\tanh(\frac{z_2}{\upsilon})\hat{\sigma} + k_{a2}e_2\end{aligned} \tag{42}$$

where $k_2 > 0$, k_{a2} is a positive constant.

To settle the estimation error of σ, the adaptive law is introduced. Moreover, the updating law of $\hat{\sigma}$ is given as

$$\dot{\hat{\sigma}} = \gamma_f(m_{33}z_2\tanh(\frac{z_2}{\upsilon}) - \gamma_\sigma\hat{\sigma}) \tag{43}$$

with $\gamma_\sigma > 0$.

Form Equations (41, 42, 43), (40) becomes

$$\begin{aligned}\dot{V}_2 &\le -(k_1 - 0.5k_{a1})z_1^{\,2} - (k_{e1} - 1)e_1^{\,2} - k_2z_2^{\,2} - k_{e2}e_2^{\,2} + z_2z_3 + k_{a2}z_2e_2 \\ &\quad + m_{33}\kappa\upsilon\sigma + m_{33}z_2\tanh(\frac{z_2}{\upsilon})\sigma - m_{33}z_2\tanh(\frac{z_2}{\upsilon})\hat{\sigma} \\ &\quad + \tilde{\sigma}(m_{33}z_2\tanh(\frac{z_2}{\upsilon}) - \gamma_\sigma\hat{\sigma}) - 0.5\gamma_2^{\,2}\Delta\alpha_2^{\,2} + e_2\gamma_2\Delta\alpha_2 \\ &= -(k_1 - 0.5k_{a1})z_1^{\,2} - (k_{e1} - 1)e_1^{\,2} - k_2z_2^{\,2} - k_{e2}e_2^{\,2} + z_2z_3 \\ &\quad + m_{33}\kappa\upsilon\sigma - 0.5\gamma_2^{\,2}\Delta\alpha_2^{\,2} - \gamma_\sigma\tilde{\sigma}\hat{\sigma} + k_{a2}z_2e_2 + e_2\gamma_2\Delta\alpha_2\end{aligned} \tag{44}$$

Based on the Definition 1, it follows that

$$e_2\gamma_2\Delta\alpha_2 \le 0.5e_2^{\,2} + 0.5\gamma_2^{\,2}\Delta\alpha_2^{\,2} \tag{45}$$

$$k_{a2}z_2e_2 \le 0.5k_{a2}^{\,2}z_2^{\,2} + 0.5e_2^{\,2} \tag{46}$$

$$-\tilde{\sigma}\hat{\sigma} = -\tilde{\sigma}(\sigma + \tilde{\sigma}) \le -\tilde{\sigma}^2 + 0.5\sigma^2 + 0.5\tilde{\sigma}^2 = -0.5\tilde{\sigma}^2 + 0.5\sigma^2 \tag{47}$$

Substituting Equations (45- 47) into (44) results in

$$\begin{aligned}\dot{V}_2 \le & -(k_1-0.5k_{a1})z_1{}^2-(k_2-0.5k_{a2})z_2{}^2-(k_{e1}-1)e_1{}^2-(k_{e2}-1)e_2{}^2 \\ & -0.5\gamma_\sigma\tilde{\sigma}^2+z_2z_3+m_{33}\kappa\upsilon\sigma+0.5\gamma_\sigma\sigma^2\end{aligned} \tag{48}$$

Step 3: denote a bounded signal ϑ as $\vartheta=\dfrac{\partial g(\varphi)}{\partial\varphi}=\begin{cases}\dfrac{4}{(e^{\frac{\varphi}{\mathrm{sign}(\varphi)\tau_M}}+e^{-\frac{\varphi}{\mathrm{sign}(\varphi)\tau_M}})^2}, & \varphi\neq 0\\ 1, & \varphi=0\end{cases}$,

then Equation (24) becomes

$$\dot{z}_3=\vartheta(-c\varphi+\phi)-\dot{\alpha}_2 \tag{49}$$

Normally, calculating ϑ^{-1} is unavoidable by using the usual method following step. To simplify design and analysis, the Nussbaum function is considered as [31]

$$\begin{cases}N(\eta)=(e^{\eta}+e^{-\eta})\cos(\dfrac{\pi}{2}\eta)\\ \dot{\eta}=\gamma_\eta\bar{\phi}z_3\end{cases} \tag{50}$$

where γ_η is a positive constant.

Define the following Lyapunov candidate function:

$$V_3=V_2+0.5z_3{}^2 \tag{51}$$

Differentiating Equation (51) and inserting (49) yields

$$\begin{aligned}\dot{V}_3=&\dot{V}_2+z_3(\vartheta(-c\varphi+\phi)-\dot{\alpha}_2)\\ \le & -(k_1-0.5k_{a1})z_1{}^2-(k_2-0.5k_{a2})z_2{}^2-(k_{e1}-1)e_1{}^2-(k_{e2}-1)e_2{}^2\\ & -0.5\gamma_\sigma\tilde{\sigma}^2+z_2z_3+m_{33}\kappa\upsilon\sigma+0.5\gamma_\sigma\sigma^2+z_3(\vartheta(-c\varphi+\phi)-\dot{\alpha}_2)\end{aligned} \tag{52}$$

We design the auxiliary signal ϕ as

$$\begin{cases}\phi=N(\eta)\bar{\phi}\\ \dot{\bar{\phi}}=-k_3z_3-z_2+c\vartheta\varphi+\dot{\alpha}_2\end{cases} \tag{53}$$

with $k_3>0$.

Substituting Equation (53) into (52) leads to

$$\begin{aligned}\dot{V}_3 &\le -(k_1-0.5k_{a1}){z_1}^2-(k_2-0.5k_{a2}){z_2}^2-(k_{e1}-1){e_1}^2-(k_{e2}-1){e_2}^2\\ &\quad -0.5\gamma_\sigma\tilde{\sigma}^2+z_2z_3+m_{33}\kappa\upsilon\sigma+0.5\gamma_\sigma\sigma^2+z_3(\vartheta\phi-k_3z_3-z_2-\bar{\phi})\\ &=-(k_1-0.5k_{a1}){z_1}^2-(k_2-0.5k_{a2}){z_2}^2-k_3{z_3}^2-(k_{e1}-1){e_1}^2-(k_{e2}-1){e_2}^2\\ &\quad -0.5\gamma_\sigma\tilde{\sigma}^2+m_{33}\kappa\upsilon\sigma+0.5\gamma_\sigma\sigma^2+z_3(\vartheta N(\eta)-1)\bar{\phi}\\ &=-(k_1-0.5k_{a1}){z_1}^2-(k_2-0.5k_{a2}){z_2}^2-k_3{z_3}^2-(k_{e1}-1){e_1}^2-(k_{e2}-1){e_2}^2\\ &\quad -0.5\gamma_\sigma\tilde{\sigma}^2+m_{33}\kappa\upsilon\sigma+0.5\gamma_\sigma\sigma^2+\frac{\dot{\eta}}{\gamma_\eta}(\vartheta N(\eta)-1)\\ &\le -\gamma V_3+d_f+\frac{\dot{\eta}}{\gamma_\eta}(\vartheta N(\eta)-1)\end{aligned} \tag{54}$$

where

$$\gamma=\min\left\{2(k_1-0.5k_{a1}),2(k_{e1}-1),\frac{2}{m_{33}}(k_2-0.5k_{a2}),2(k_{e2}-1),\gamma_\sigma\gamma_f,2k_3\right\},$$

$d_f=m_{33}\kappa\upsilon\sigma+0.5\gamma_\sigma\sigma^2$.

Integrating Equation (47) directly, the following inequality has the following performance:

$$0\le V_3(t)\le V_3(0)\,\mathrm{e}^{-\gamma t}+\frac{d_f}{\gamma}(1-\mathrm{e}^{-\gamma t})+\frac{\mathrm{e}^{-\gamma t}}{\gamma_\eta}\int_0^t(\vartheta\mathrm{N}(\eta)-1)\dot{\eta}e^{\gamma\tau}d\tau \tag{55}$$

With the Lemma 2, $V_3(t)$ and η are bounded.

Using the definition of UUB stability [32], which expresses final state of the control system is properly governed to converge to a small ball centered at the origin. It can be thus concluded from (55) that V_3 is UUB together with the states $z_i(i=1,2,3)$, which means for any $\delta>0$ (δ is a small constant), there exists a positive value of finite time T such that $|z_i(t)|<\delta(i=1,2,3)$ with $t>T$, specifically.

Then, it leaves the new heading error as

$$|e_a|=|\psi-\psi_{da}|=|\psi-\psi_d+\beta|=|z_1|<\delta,t>T \tag{56}$$

It implies that e_a is UUB.

The control laws ϕ and $\bar{\phi}$ both are bounded because of the boundedness of the error states $z_i(i=1,2,3)$. The control laws $\alpha_{i0}(i=1,2)$ and the corresponding α_i from the command filter both are bounded. And the states $e_i(i=1,2)$ of the auxiliary system and the estimation error of σ are all bounded. In addition, other aforementioned signals are bounded.

Consequently, choosing appropriate controller parameter values $k_i(i=1,2,3)$, $k_{ei}(i=1,2)$, $k_{ai}(i=1,2)$, c, γ_f and γ_σ, then the heading error can be converge to a smaller value. All signals are bounded in the closed loop system. And the adaptive law (43) can estimate and compensate the bounded external disturbances robustly. Under the proposed control techniques, the desired heading can be followed accurately with a smaller control input.

5. Simulations

In this section, to verify the effectiveness of the proposed controller, several studies are carried out. We choose a 2-DOF nonlinear mathematical model of the underactuated vessel with yaw, surge and sway as the simulation object. The vessel parameters are taken from [33], as shown in Tab.1. The yaw motion disturbance model is given by (6) and (7), and the parameters are presented in Tab.2.

Tab.1 Parameters of the ship model parameters

m_i / kg $(i=11,22,33)$	d_{vi} / kg·s^{-1} $(i=1,2,3)$	d_{ri} / kg·s^{-1} $(i=1,2,3)$	λ	τ_M / Nm
120×10^3, 172.9×10^3, 636×10^5	147×10^3, $0.2d_{v1}$, $0.1d_{v1}$	802×10^4, $0.2d_{r1}$, $0.1d_{r1}$	0.01	1.5×10^7

Tab.2 Parameters of the yaw disturbance model

T_ω / s	$h_{1/3}$ / m	ς	K_ω	σ_m	ω_0	f / Hz
8	3	0.3	0.42	1.154	0.606	0.1

The external disturbances affecting the sway velocity are chosen as $\omega_{v1}=(26/17.79)(1+0.3\cos(0.4t))$, $\omega_{v2}=-(950/636)(1+0.3\cos(0.3t))$.

The designed parameters of the heading controller and the command filter are specified in Tabs.3 and 4, respectively.

Tab.3 Design parameters of the heading controller

k_1	k_2	k_3	$k_{a1}=k_{a2}$	$k_{e1}=k_{e2}$	c	$\bar{e}_1=\bar{e}_2$	$\gamma_1=\gamma_2$	γ_f	γ_σ	γ_η
0.83	1	50	0.01	10	1	0.01	0.1	1	1	10^{-3}

Tab.4 Design parameters of the command filter

ξ_1	ξ_2	ω_1	ω_2	α_{10m}	α_{11m}	α_{20m}	α_{21m}
1.1	1.1	10	50	10	10	30	30

The vessel is sailing with a speed of $10\,\mathrm{m/s}$ and following the desired heading angle given as 30°, 60° and 120°, respectively.

This paper compares the simulation results of the proposed controller with constrained input and sideslip angle compensation (A-BAWIC), the traditional backstepping controller (T-B) and the backstepping controller with sideslip angle compensation (A-B). And the latter two controllers do not deal with input saturation constraints. The corresponding initial conditions and related parameters are maintained with the same values in the simulation of three models. All simulation results are shown below which are divided into two parts: the heading angle and the rudder moment. T-desired represents the desired heading.

5.1 The heading angle and the corresponding error

The steady state error of the heading angle is affected by the sideslip angle, which is related to many reasons, such as the vessel sway speed, current velocity and so on.

Considering the above factors and the balance between the control input and output, the current velocity and azimuth with respect to the earth fixed frame are given as $V_c = 1\text{m/s}$ and $\beta_c = 10^\circ$.

The simulation results of the output heading angle and corresponding errors of different controllers are shown in Figs.4 and 5. When the course is changing, the output errors are all very large, as shown in Fig.5. The overshoot is large, because of the sudden course changing. Due to the irrationality of desired heading, it can be seen that the heading error cannot converge to zero. A-BAWIC can ensure that the system tends to be stable within 3-5 seconds and the overshoot is reduced by more than 90%. In the stable state, the heading error of A-BAWIC is $1^\circ \sim 2^\circ$ more accurate than that of T-B, as shown in Fig.4. In other words, by comparing with the other controllers, A-BAWIC can improve the performance of the vessel heading control and reduce the heading error effectively; it also can restrain the overshoot of the system in a shorter time.

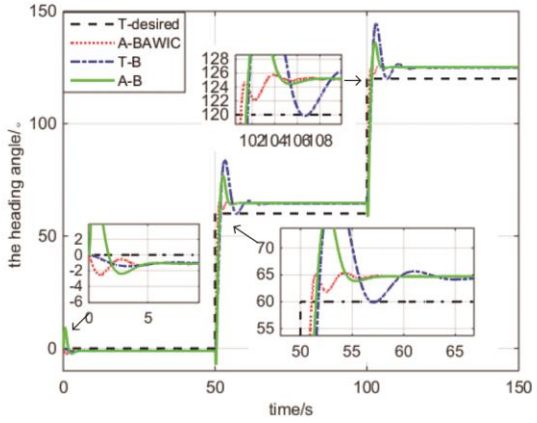

Fig. 4 The heading angles of the controllers

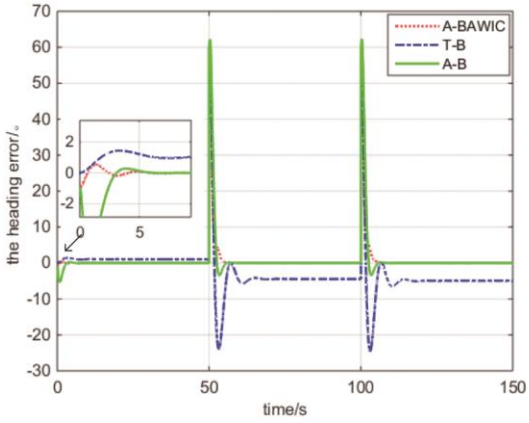

Fig. 5 The heading errors of the controllers

5.2 The control input (the rudder moment)

Besides parameters $k_i (i = 1,2,3)$, other parameters can also affect the control performance. In the process of simulation debug, the chosen of larger $k_{ei} (i = 1,2)$ and γ_σ choose can lead to the smaller the heading error, but the control input is larger simultaneously. Excessive control input (rudder moment) will increase the wear and tear of the rudder servo system. Therefore, the control parameters are given carefully (i.e. $k_{e1} = k_{e2} = 10$, $\gamma_f = \gamma_\sigma = 1$) to cope with the trade-off between the heading performance and the saturation constraint.

Fig.6 presents the simulation results about the control input. It can be founded that rudder moments without constraints are large when the heading is changing. Especially, the input of A-B exceeds the operation condition of the rudder. To solve this problem, A-BAWIC is designed to limit the control input before the control commands are putted on the actuators. In Fig.7, The average of the rudder moment of A-BAWIC in the range of $(-2 \sim 2)\text{Nm}$, which is 1.33×10^{-7} of the saturation limit. Even the maximum rudder moment of A-BAWIC does not exceed 8Nm. And it is much smaller than these of T-B and A-B whether the desired heading is changing or not.

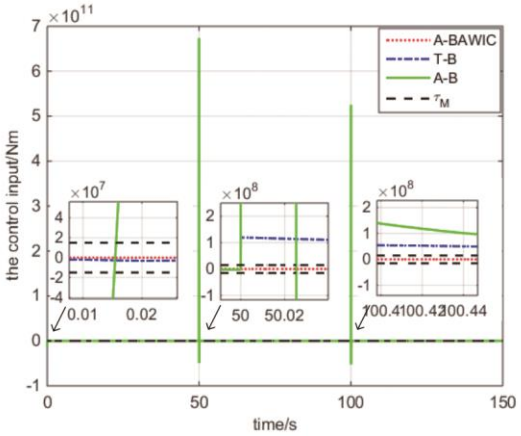

Fig. 6 The rudder moment of the controllers

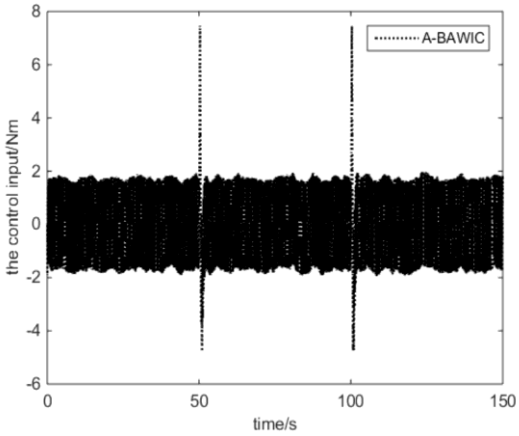

Fig. 7 The rudder moment of the controller A-BAWIC

Tab.5 Control effect comparison between different control methods

Type	Rising time / s	settling time / s	Overshoot /%	Heading error /(°)	The maximum rudder moment / Nm
A-BAWIC	2	4	1.5	1	7.8
T-B	3	13	23	3.6	1.2×10^{8}
A-B	2.8	4.5	23	1	6.7×10^{11}

In Tab.5, the maximum rudder moments are the absolute value, others are the average absolute values.

6. Conclusion

Based on the backstepping technique, a constructive method has been proposed to solve the heading control problem for an underactuated surface vessel with input saturation and sideslip angle in this paper. The undifferentiable input saturation was approximated by hyperbolic tangent function and Nussbaum function, which satisfied the requirement of the backstepping method for continuous functions. The command filter simplified the derivation calculation of virtual control law. Finally, the simulation studies verified the proposed controller can effectively improve the heading control performance of the underactuated vessel with a small rudder moment. However, it should be pointed out that the surface vessel model is simplified. The nonlinear dynamics and uncertain parameters of the vessel can be fully considered in the future research. Furthermore, the overshoot is large when the heading is changed, so the authors plan to use the pre-filter method to improve the tracking accuracy in the future work.

ACKNOWLEDGEMENTS

This work was supported by National Natural Science Foundation of China (51839004), International Academic Cooperation and Exchange Project of Shanghai (18550720100) and Capacity Building Project of Shanghai Local Colleges and Universities (19040501600).

REFERENCES

[1] Dai, S. L., Wang, M. and Wang, C., 2016, “Neural Learning Control of Marine Surface Vessels with Guaranteed Transient Tracking Performance,” IEEE Transactions on Industrial Electronics, 63(3), pp. 1717-1727. https://doi.org/10.1109/TIE.2015.2504553

[2] Zhang, G., Deng, Y. and Zhang, W., 2017, "Robust Neural Path-following Control for Underactuated Ships with the DVS Obstacles Avoidance Guidance," Ocean Engineering, 143, pp. 198-208. https://doi.org/10.1016/j.oceaneng.2017.08.011

[3] Zhang, X. and Zhang, G., 2016, "Design of Ship Course-Keeping Autopilot using a Sine Function-Based Nonlinear Feedback Technique," Journal of Navigation, 69(2), pp. 246-256. https://doi.org/10.1017/S0373463315000612

[4] Yin, S., Shi, P. and Yang, H., 2011, "Adaptive Fuzzy Control of Strict-feedback Nonlinear Time-delay Systems with Unmodeled Dynamics," IEEE Transactions on Cybernetics, 46(8), pp. 1926–1938. https://doi.org/10.1109/TCYB.2015.2457894

[5] Yin, S., Yu, H., Shahnazi, R., et al. 2017, "Fuzzy Adaptive Tracking Control of Constrained Nonlinear Switched Stochastic Pure-Feedback Systems," IEEE Transactions on Cybernetics, 47, pp. 579-588. https://doi.org/10.1109/TCYB.2016.2521179

[6] Dlabač, T., Alasan M., Krum M., et al. 2019, "Pso-based PID controller design for ship course-keeping autopilot," Brodogradnja, 70(4), pp. 1-15. https://doi.org/10.21278/brod70401

[7] Huang, H., Sharma, S., Zhuang, Y., et al. 2017, "Dynamic Positioning of an Uninhabited Surface Vehicle Using State-dependent Riccati Equation and Pseudospectral Method," Ocean Engineering, 133, pp. 215-223. https://doi.org/10.1016/j.oceaneng.2017.02.004

[8] Yin, S. and Xiao, B., 2017, "Tracking Control of Surface Ships with Disturbance and Uncertainties Rejection Capability," IEEE/ASME Transactions on Mechatronics, 22, pp. 1154-1162. https://doi.org/10.1109/TMECH.2016.2618901

[9] Anna, W., Smierzchalski, R., 2018, "Adaptive Dynamic Control Allocation for Dynamic Positioning of Marine Vessel based on Backstepping Method and Sequential Quadratic Programming," Ocean Engineering, 163, pp. 570-582. https://doi.org/10.1016/j.oceaneng.2018.05.061

[10] Wen, G. X., Sam, G. S., Philip, C. C. L., et al. 2019, "Adaptive Tracking Control of Surface Vessel Using Optimized Backstepping Technique," IEEE Transactions on Cybernetics, 49(9), pp. 3420-3431. https://doi.org/10.1109/TCYB.2018.2844177

[11] Fossen, T. I., Pettersen, K. Y. and Galeazzi, R., 2015, "Line-of-Sight Path Following for Dubins Paths with Adaptive Sideslip Compensation of Drift Forces," IEEE Transactions on Control Systems Technology, 23(2), pp. 820-827. https://doi.org/10.1109/TCST.2014.2338354

[12] Ma, J., Ge, S. S., Zhang, Z., et al. 2015, "Adaptive NN Control of a Class of Nonlinear Systems with Asymmetric Saturation Actuators," IEEE Transactions on Neural Networks and Learning Systems, 26(7), pp. 1532-1538. https://doi.org/10.1109/TNNLS.2014.2344019

[13] Shahnazi, R., 2016, "Observer-based Adaptive Interval Type-2 Fuzzy Control of Uncertain MIMO Nonlinear Systems with Unknown Asymmetric Saturation Actuators," Neurocomputing, 171, pp. 1053-1065. https://doi.org/10.1016/j.neucom.2015.07.098

[14] Yu, C., Xiang, X., Wilson, P. A., et al. 2020, "Guidance-error-based Robust Fuzzy Adaptive Control for Bottom Following of a Flight-style AUV with Saturated Actuator Dynamics," IEEE Transactions on Cybernetics, 50(5), pp. 1887-1899. https://doi.org/10.1109/TCYB.2018.2890582

[15] Du, J., Hu, X., Miroslav, K., et al. 2016, "Robust Dynamic Positioning of Ships with Disturbances under Input Saturation," Automatica, 73, pp. 207-214. https://doi.org/10.1016/j.automatica.2016.06.020

[16] Wang, Y., Chai, S., Khan, F., et al. 2017, "Unscented Kalman Filter Trained Neural Networks based Rudder Roll Stabilization System for Ship in Waves," Applied Ocean Research, 68, pp. 26-38. https://doi.org/10.1016/j.apor.2017.08.007

[17] Liu, L., Wang, D. and Peng, Z., 2017, "ESO-Based Line-of-Sight Guidance Law for Path Following of Underactuated Marine Surface Vehicles With Exact Sideslip Compensation," Oceanic Engineering, 42(2), pp. 477-487. https://doi.org/10.1109/JOE.2016.2569218

[18] Peng, Z. H. and Wang, J., 2018, "Output-Feedback Path-Following Control of Autonomous Underwater Vehicles Based on an Extended State Observer and Projection Neural Networks," IEEE Transactions on Systems, Man, and Cybernetics: Systems, 48(4), pp. 535-544. https://doi.org/10.1109/TSMC.2017.2697447

[19] Tchamna, R , Youn, I., 2013, "Yaw Rate and Side-slip Control Considering Vehicle Longitudinal Dynamics," International Journal of Automotive Technology, 14(1), pp.53-60. https://doi.org/10.1007/s12239-013-0007-1

[20] Lin, X., Nie, J., Jiao, Y., et al. 2018, "Nonlinear Adaptive Fuzzy Output-feedback Controller Design for Dynamic Positioning System of Ships," Ocean Engineering, 158, pp. 186-195. https://doi.org/10.1016/j.oceaneng.2018.03.086

[21] Nie, J. and Lin, X. G., 2020, "FAILOS Guidance Law Based Adaptive Fuzzy Finite-time Path Following Control for Underactuated MSV," Ocean Engineering, 195, 106726. https://doi.org/10.1016/j.oceaneng.2019.106726

[22] Yu, Z., Bao, X. and Nonami, K., 2008, "Course Keeping Control of an Autonomous Boat using Low Cost Sensors," Journal of System Design and Dynamics, 2(1), pp. 389-400. https://doi.org/10.1299/jsdd.2.389

[23] Li, J. H., Lee, P. M., Jun, B. H., et al. 2008, "Point-to-point Navigation of Underactuated Ships," Automatica, 44(12), pp. 3201-3205. https://doi.org/10.1016/j.automatica.2008.08.003

[24] Li, Z., Sun, J. and Oh, S., 2009, "Design, Analysis and Experimental Validation of a Robust Nonlinear Path Following Controller for Marine Surface Vessels," Automatica, 45(7), pp. 1649-1658. https://doi.org/10.1016/j.automatica.2009.03.010

[25] Do, K. D., 2016, "Global Robust Adaptive Path-tracking Control of Underactuated Ships under Stochastic Disturbances," Ocean Engineering, 111, pp. 267-278. https://doi.org/10.1016/j.oceaneng.2015.10.038

[26] Wang, H., Chen, B., Liu, X., et al. 2013, "Robust Adaptive Fuzzy Tracking Control for Pure-Feedback Stochastic Nonlinear Systems with Input Constraints," IEEE Transactions on Cybernetics, 43(6), pp. 2093-2104. https://doi.org/10.1109/TCYB.2013.2240296

[27] Polycarpou, M. M. and Ioannou, P. A., 1996, "A robust adaptive nonlinear control design," Automatica, 32(3), pp. 423-427. https://doi.org/10.1016/0005-1098(95)00147-6

[28] Wen, C., Zhou, J., Liu, Z., et al. 2011, "Robust Adaptive Control of Uncertain Nonlinear Systems in the Presence of Input Saturation and External Disturbance," IEEE Transactions on Automatic Control, 56(7), pp. 1672-1678. https://doi.org/10.1109/TAC.2011.2122730

[29] Hu, C., Wang, R., Yan, F., et al. 2016, "Robust Composite Nonlinear Feedback Path-Following Control for Underactuated Surface Vessels with Desired-Heading Amendment," IEEE Transactions on Industrial Electronics, 63(10), pp. 6386-6394. https://doi.org/10.1109/TIE.2016.2573240

[30] Chen, M., Ge, S. S. and Ren, B., 2011, "Adaptive Tracking Control of Uncertain MIMO Nonlinear Systems with Input Constraints," Automatica, 47(3), pp. 452-465. https://doi.org/10.1016/j.automatica.2011.01.025

[31] Zhang, Z., Huang, Y., Xie, L., et al. 2018, "Adaptive Trajectory Tracking Control of a Fully Actuated Surface Vessel with Asymmetrically Constrained Input and Output," IEEE Transactions on Control Systems Technology, 26(5), pp. 1851-1859. https://doi.org/10.1109/TCST.2017.2728518

[32] Khalil, H. K., 2002, Nonlinear Systems. Prentice-Hall, Upper Saddle River, NJ, USA, Chap. 3.

[33] Chwa, D., 2011, "Global Tracking Control of Underactuated Ships with Input and Velocity Constraints Using Dynamic Surface Control Method," IEEE Transactions on Control Systems Technology, 19(6), pp. 1357-1370. https://doi.org/10.1109/TCST.2010.2090526

Submitted: 10.10.2019.
Accepted: 01.09.2020.

Xiaoyang Lu, 723963224@qq.com
Zhiquan Liu (the corresponding author), liuzhiquan215@sina.com
Key Laboratory of Marine Technology and Control Engineering Ministry of Communications, Shanghai Maritime University, Shanghai 201306, China
Zhenzhong Chu, chu_zhenzhong@163.com
Logistics Engineering College, Shanghai Maritime University, Shanghai 201306, China